JMEPEG (2009) 18:190–195
DOI: 10.1007/s11665-008-9281-x

1059-9495/$19.00

The Influence of Corrosion and Cross-Section Diameter on the Mechanical Properties of B500$_c$ Steel

Ch. Alk. Apostolopoulos

(Submitted February 6, 2008; in revised form July 3, 2008)

Corrosion is a negative contributor on the structural integrity of concrete structures and leads to degradation of the mechanical properties of steel rebar. Exposure to chloride, seawater, salt and saltwater and deicing chemical environments influences the concrete-steel bond and weakens it. A considerable strength factor of the two-phase steel B500$_c$ (martensitic, ferritic-perlitic) is considered to be the outer martensitic cortex thickness, which varies according to the area of the rebar cross section. In order to evaluate the influence of corrosion and the size of the area on the mechanical properties of B500$_c$ steel, an experimental investigation was conducted on B500$_c$ ribbed steel rebar of 8, 12, 16, and 18 mm diameter, and which were artificially corroded for 10, 20, 30, 45, 60, 90, and 120 days. The laboratory tests suggest that corrosion duration and rebar cross-sectional area size had a significant impact on the strength and ductility degradation of the specimens. The tensile mechanical properties before and after corrosion indicated progressive variation and drastic drop in their values. The extended salt spray exposure enhanced the damage and created pits and notches, resulting in stress concentration points and progressive reduction of ductility and available energy. Anti-seismic design and codes that ignore the influence of the size of the cross-section area and the level of corrosion and mechanical behavior of reinforcing steel could lead to unpredictable performance during severe ground motion.

Keywords artificial corrosion, cross section of B500$_c$ steel rebar, degradation of mechanical properties

1. Introduction

Steel rebar corrosion appears to be the main reason for structural concrete degradation; it constitutes a serious problem in seismic areas and is a serious safety and economic issue.

The high pH level of the concrete pore solution provides protection to the reinforcing steel, by forming a thin oxide passive layer covering the reinforcement. This layer remains stable in the alkaline concrete environment of pH 12.5-13, but begins to deteriorate when the pH of the pore solution drops below 11 (Ref 1, 2). The corrosion rate rises when the pH drops under 9. For corrosion to commence, the oxide film must be broken or de-passivated, which may occur if the alkalinity of the pore water in the concrete pores decreases and/or penetration of the chloride ions takes place. This may be caused by carbonation, especially in the proximity of cracks, or by water dilution, which accompanies cracking (Ref 3, 4).

The advancing corrosion results in reduction of the load carrying cross section of the bars and an increase of their volume by 3-8 times, which in turn causes the build-up of internal stresses with eventual cracking and spalling of the concrete cover, leading to further corrosion escalation (Ref 5, 6). Usually the layer of corrosion products consists of water and hydrated iron oxides, which due to their volumetric expansion develop cracks in the concrete leaving the reinforcing steel unprotected to corrosion (Ref 7).

The climatic conditions in locations near the sea constitute one of the most aggressive environments for concrete structures due to the high ambient salinity, temperature and humidity and also due to the ingress of chlorine through wind-borne salt. Chloride-induced damage of reinforcing steel results in concrete cracking and spalling, destruction of the protective steel barrier and formation of pits, notches and cavities on the steel surface. The chlorides within the salt act as a catalyst in the natural corrosion process. Once corrosion commences, the reinforcement is eventually replaced by rust, a porous product of higher volume than the steel which exerts tensile forces on the surrounding concrete, thus inducing delamination along the interface between steel and concrete (Ref 8).

The reduction in the structural performance of reinforced concrete members due to corroded steel is caused by the loss in the effective cross-sectional area of concrete due to cracking in the cover concrete, loss in bonding (Ref 6, 9, 10), loss in the mechanical properties and performance of reinforcing bars due to reduction of their cross-sectional area, and development of pits and notches which are responsible for the development of stress concentration points. An attempt to quantify corrosion and mass loss of steel with the reduction of its mechanical properties has been made (Ref 11-15).

It is known that the powerful external martensitic skin is responsible for the strength characteristic properties of B500$_c$ steel, while its ductility depends on the soft kernel. It has also been verified that the strength and ductility properties of steel are greatly reduced by corrosion and at some instant of time they drop under the minimum code limits (Ref 11, 14).

Ch. Alk. Apostolopoulos, Department of Mechanical Engineering and Aeronautics, University of Patras, Patras 26500, Greece. Contact e-mail: charrisa@mech.upatras.gr.

Rebar corrosion is of paramount importance in seismic areas, since during strong earthquake activity the requirement for structures with high ductility is necessary. Steel corrosion, combined with tensile and compressive stresses, the predisposition of the material for fracture, the level of corrosive atmosphere, and the size of the implied mechanical stresses, leads eventually in fracture (Ref 16). The result of such a combination may be the fast degradation and failure of the material. Even though the impact of corrosion on the strength of steel reinforcing bars is well known, the current design codes do not face the problem since they are unable to quantify it and need further review (Ref 17-20, 22).

The necessity for reliable and predictable mechanical performance of reinforcing steel, on a long-term basis, must be the on-going target of every construction project. Besides the corrosion factor, however, there has also been realized some degree of variation in the mechanical properties of the non-corroded $B500_c$ steel and the size of its cross-section area. Even though there is no literature backing such an allegation, the present study was conducted in order to verify the impact of corrosion duration and size of cross-sectional area on the tensile mechanical properties of $B500_c$ steel, and in the general mechanical behavior.

2. Experimental Procedure

2.1 Induced Corrosion

In the present study, ribbed $B500_c$ steel rebar was used with rebar diameters of 8, 12, 16, and 18 mm which were artificially corroded for 10, 20, 30, 45, 60, 90, and 120 days. The tensile specimens were cut and prepared in lengths of 436, 488, 544, and 572 mm, which left a clear length between grips of 316, 368, 424, 452 mm, in addition to 60 mm length in either side. The specimens were artificially corroded in a specially designed salt spray corrosion chamber, according to ASTM B117-94 standard. Prior to corrosion, the specimens were measured and weighed with accuracy of 0.01 g.

The corrosion process was accelerated by spraying the specimens with a 5% sodium chloride and 95% distilled water solution, with pH range of 6.5-7.2 and spray chamber temperature of $35\pm^{1.1}_{1.7}$ °C for different exposure durations so that different corrosion levels were obtained. The surface thickness variation of the martensite before and after the salt spray corrosion process appeared to be higher in the location of the ribs and lower in between them. Pitting was observed to have started progressively on the specimens after 10, 20, and 30 days corrosion level which became progressively more severe. After salt spray exposure, the specimens were washed with clean water according to ASTM G 1-72 in order to remove any residual salt deposits from their surface. The rebar samples were then dried.

Six specimens from each diameter were exposed to salt spray for 10, 20, 30, 45, 60, 90, and 120 days, respectively, in order to monitor the evolution of corrosion damage and establish a relationship between duration to salt spray exposure and corrosion level. After each corrosion process, the specimens were cleaned, weighed, and the mass loss was calculated according to ASTM G1-90. The tensile tests that followed were conducted according to ISO 15630-1, at 24 °C, using a strain rate of 2 mm/min. The stress was calculated according to DIN 488-3, and the area was

$$A_s = \frac{1.274 \times M_f}{l} \quad \text{(Eq 1)}$$

where M_f is the final mass and l is the bar length.

A total of 192 successful tests were performed, 6 per each diameter and each corrosion level. The mechanical properties that were evaluated included the nominal $R_{p\text{-}nom}$ (MPa) and effective $R_{p\text{-}eff}$ (MPa) yield stress, the nominal $R_{m\text{-}nom}$ (MPa) and effective $R_{m\text{-}eff}$ (MPa) ultimate stress, the uniform elongation A_{gt} (%), and the energy density U (N/mm^2), which was calculated from the area under the stress-strain curve, using the real (effective) cross-sectional area of the steel specimens. The nominal yield stress is calculated as the ratio of the load capacity divided by the initial non-corroded cross-sectional area of the steel bars. The effective yield stress is the ratio of the load capacity divided by the true cross-sectional area of the corroded specimens, which was calculated as a function of the mass and length of each specimen.

According to ELOT 1421-1 (Ref 22), the chemical composition of $B500_c$ steel in maximum by weight permissible values is C = 0.24, S = 0.055, P = 0.055, N = 0.014, and Cu = 0.85, and the equivalent carbon content Ceq was determined to be 0.52. The material yield stress is ≥ 500 (MPa); the ratio $1.15 \leq R_m/R_y \leq 1.35$; and elongation at maximum load ≥ 7.5 (%).

2.2 Mass Loss

A series of tests were conducted on 8, 10, 12, 16, and 18 mm diameter $B500_c$ ribbed steel rebar specimens in order to understand the effect of corrosion on its mass loss. The 10-mm diameter group of specimens were included additionally in order to gain a better insight for the mass loss, 6 per each corroded and non-corroded level, or a total of 48 tests.

The corrosion level was measured as the percentage of the difference between initial and final masses before and after corrosion.

The mass loss of Table 1 is initiated in the outer steel surface and affects mainly the martensitic cortex which is directly related with the mechanical properties of the material. In order to determine the percentage of martensitic cortex thickness for each sample, stereoscopic images of the specimens were obtained from three different angles, and for 6 specimens per level of corrosion and diameter.

Table 1 Percentage mass loss of different nominal diameters and different corrosion levels of $B500_c$ steel specimens

Duration, days	Nominal diameter, mm				
	8	10	12	16	18
0	0.00	0.00	0.00	0.00	0.00
10	1.33	1.00	0.92	0.94	0.67
20	2.67	2.19	1.77	0.99	1.21
30	3.03	2.90	2.40	2.71	1.76
45	5.15	4.28	4.01	4.77	2.01
60	6.55	5.97	5.50	5.77	3.16
90	9.89	8.52	8.93	5.14	3.95
120	13.55	11.50	11.66	7.83	5.08

Fig. 1 Stereoscopic image of specimen cross section after Nital immersion

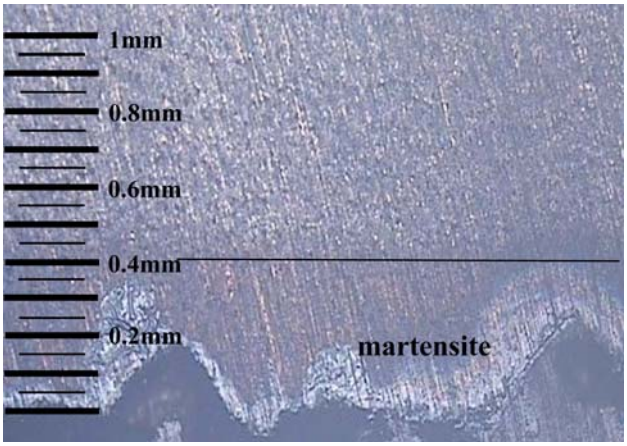

Fig. 2 Martensite transverse section cortex thickness of corroded for 90 days specimen

The steel specimens were cut and prepared in cross and transverse sections, shown in Fig. 1 and 2, in order to examine the surface thickness variation of the martensitic layer, which appears to be higher in the location of the ribs and lower in between them and also the influence of the salt spray corrosion. The preparation included sectioning/resin immersion/grinding and polishing, and Nital (1.5-5 mL of nitric acid diluted in 100 mL ethyl alcohol) was used for the chemical etching, which makes visible the martensitic cortex, while its thickness was calculated using appropriate photographic software. The remaining martensite area was calculated from Eq 2, and is depicted in Fig. 3.

$$\text{Martensite}\% = \frac{\text{Total area} - \text{Inner area}}{\text{Total area}} \times 100 \qquad \text{(Eq 2)}$$

The experimental results were fitted to an exponential decay equation of the form

$$y = y_o + A \cdot e^{-(x/t)} \qquad \text{(Eq 3)}$$

and the values of the constants y_o, A, and t are shown in Table 2.

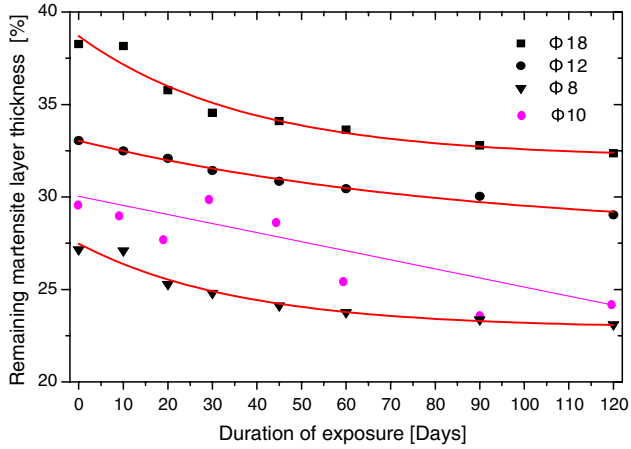

Fig. 3 Impact of corrosion on the martensitic layer thickness for 8, 10, 12, and 18 mm diameter specimens

Table 2 Exponential decay equation constants

	Martensite, %			
Constants	8 mm diameter	10 mm diameter	12 mm diameter	18 mm diameter
y_o	22.84467	−3133.6868	29.30056	32.29097
A	4.61957	3165.1900	3.87796	6.58644
t	37.18443	50759.647	51.27738	34.55036

The corrosion process created notches and cavities in the outer surface of the specimens as shown in Fig. 2, with depth measured approximately 0.40 mm after 90 days corrosion level. The roughness and crack formation in the outer surface is mostly responsible for the material's mechanical properties and ductility degradation.

In reinforced concrete structures and when steel corrosion in statically critical areas where recycling has devaluated the concrete, then the notches and cavities may become critical for the structural integrity.

Figure 3 shows that the martensitic cortex thickness increased in the bigger diameter specimens, while it was decreased exponentially as the corrosion rate increased.

3. Results

An experimental study was conducted on 8, 12, 16, and 18 mm diameter $B500_c$ ribbed steel rebar which were artificially corroded by sodium chloride spray, simulating satisfactorily the natural corrosion process. The mechanical properties were evaluated and some very interesting conclusions were drawn, as shown in Fig. 4-10. The three-dimensional figures (Fig. 4-7, 9, and 10) depict the impact of corrosion on the variation of the mechanical properties of different diameter specimens. These results were fitted to nonlinear Extreme Value and Gaussian Functions, Taylor Series Polynomials, as shown in Eq 4 and 5, and the values of the constants are shown in Table 3.

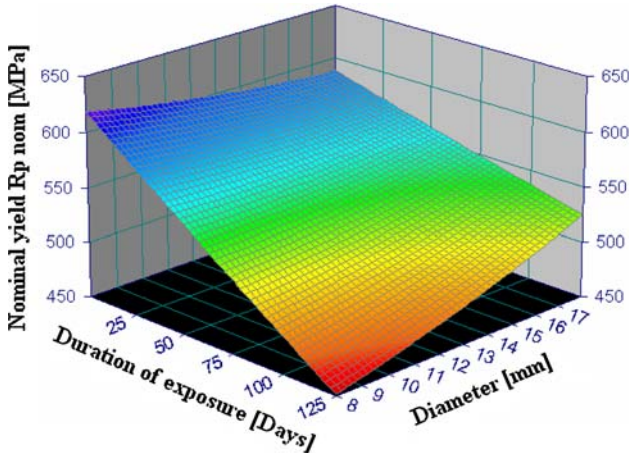

Fig. 4 Rate of change of the nominal yield stress as a function of the corrosion duration and diameter size

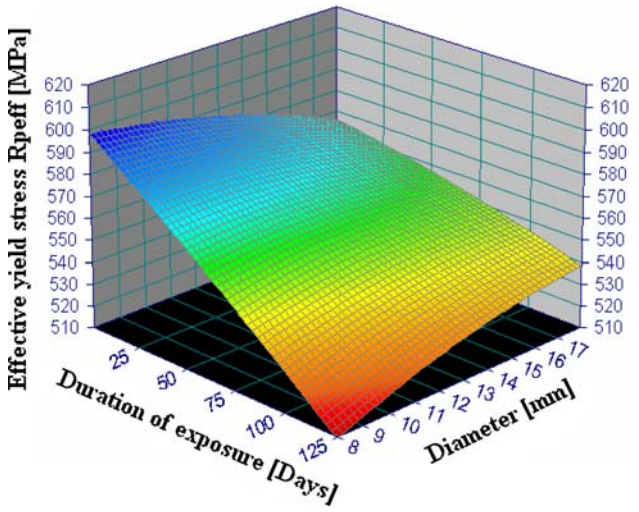

Fig. 5 Rate of change of the effective yield stress as a function of the corrosion duration and diameter size

- Taylor Series Polynomial

$$z = a + b * x + c * y + d * x^2 + e * y^2 + f * x * y \qquad \text{(Eq 4)}$$

- Non-linear Extreme Value Function

$$z = a + b * e^{-e^{-\frac{x-c}{d}} - \frac{x-c}{d} + 1} + e * e^{-e^{-\frac{y-f}{g}} - \frac{y-f}{g} + 1} + h * e^{-e^{-\frac{x-c}{d}} - \frac{x-c}{d} + 1} * e^{-e^{-\frac{y-f}{g}} - \frac{y-f}{g} + 1} \qquad \text{(Eq 5)}$$

The nominal and effective mechanical strength properties of $B500_c$ steel were calculated using the nominal and real cross-sectional area, ELOT 1421 code, and Eq 1, of the specimen.

4. Discussion

Table 1 shows that for equal salt spray duration the mass loss is indirectly proportional with the nominal specimen diameter. This is expectable since the depth of corrosion attack for equal durations is constant for all size specimens, the consequence of which is that the constant diameter reduction results in lower percentage loss of material for the bigger diameters.

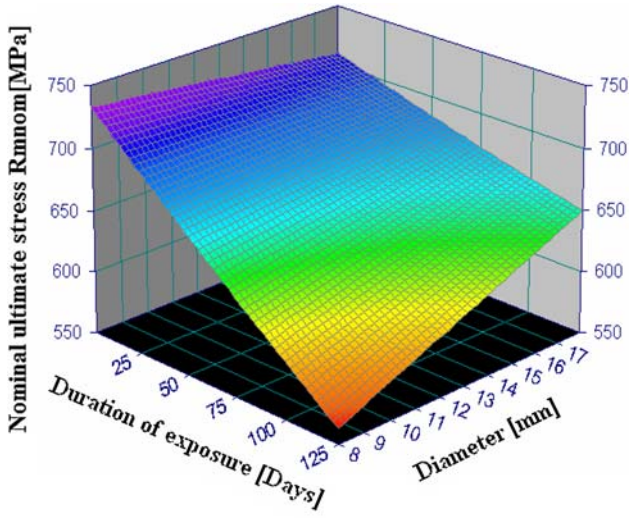

Fig. 6 Rate of change of the nominal ultimate stress as a function of the corrosion duration and diameter size

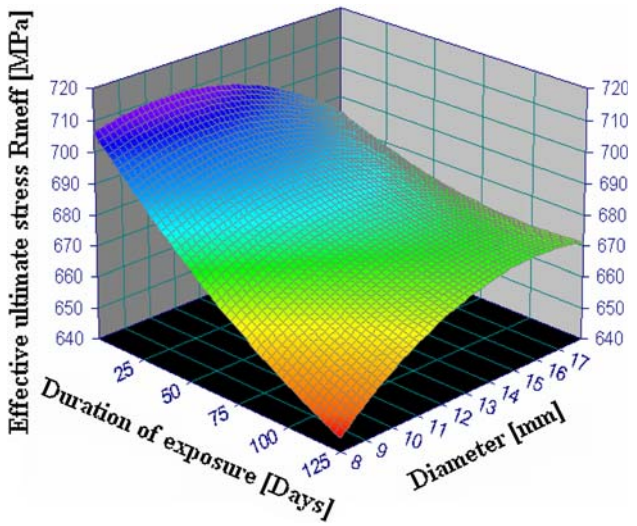

Fig. 7 Rate of change of the effective ultimate stress as a function of the corrosion duration and diameter size

Figure 3 shows a higher percentage concentration of martensite in the bigger diameters and exponential reduction as the level of corrosion increases. The martensite content for the non-corroded specimens was as follows:

Diameter, mm	8	10	12	18
Martensite content, %	25	30	32.5	38

Corrosion exposure of up to 120 days created approximately equal rate of martensite area reduction. The strength properties of $B500_c$ steel are attributed to the presence of martensite, while the ductility properties are due to the soft ferritic-perlitic core.

Figures 4-7 shows that, for the non-corroded specimens, there is a gain in the mechanical strength properties of the

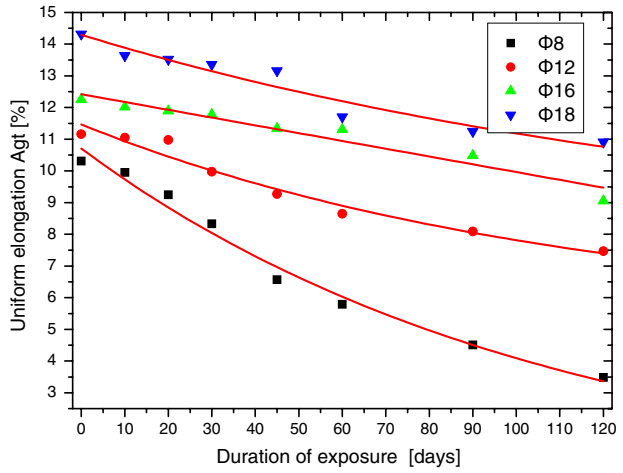

Fig. 8 Rate of change of the uniform elongation as a function of the corrosion duration and diameter size

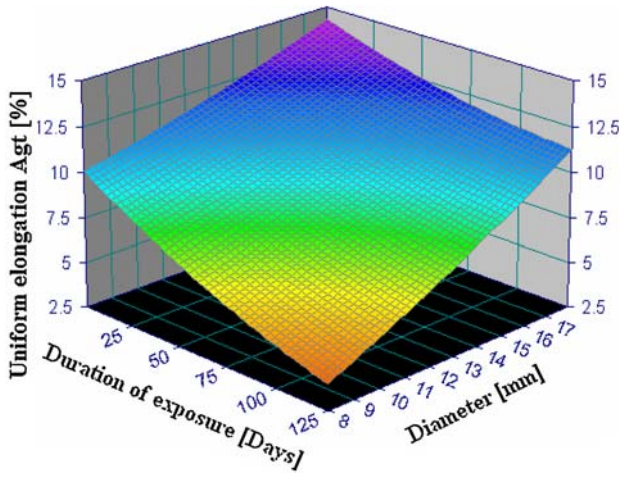

Fig. 9 Rate of change of the uniform elongation as a function of the corrosion duration and diameter size

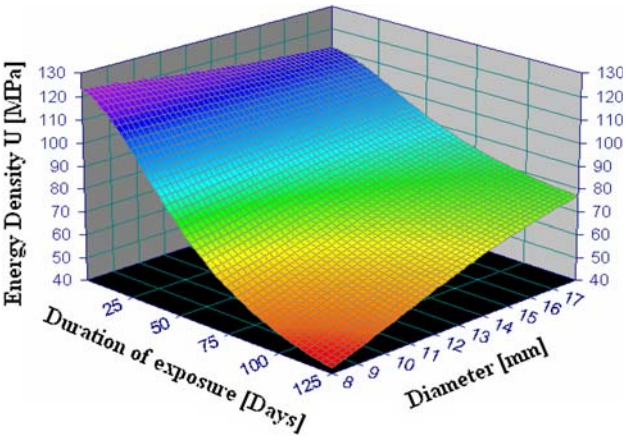

Fig. 10 Rate of change of the energy density as a function of the corrosion duration and diameter size

smaller vs. the larger diameter specimens. This is an interesting point since the martensitic content in the smaller diameters was found to be lower than in the higher diameters. This is probably due to the different behavior of the smaller diameters and the imperfections of the material surface, which as such are considered to be the ribs. It was also observed that corrosion level had a greater impact on the degradation rate of these properties for the smaller diameter specimens. This was also expected since the pits and notches that were generated due to corrosion are especially high and constitute the determining factor for the creation of stress concentration points. Therefore the mechanical behavior of the smaller diameter specimen vs. time appears to be questionable. On the other hand, the higher vs. the lower diameter specimens present higher levels of ductility.

In addition, the degradation rate of the uniform elongation and the energy density due to corrosion, for smaller diameter specimens, were found to be higher. This might have been expected since for equal corrosion durations the same amount of pits and notches that are present in the smaller diameters create greater damage, since they occupy greater percentage of surface area.

Figures 4, 8-11 indicates a variation of the limits of yield stress, uniform elongation, and energy density by 8, 40, and 19% accordingly between non-corroded rebar of 8 and 18 mm diameters. A more complex situation exists as the corrosion level increases, since from Fig. 4-11 higher degradation rates of the mechanical properties and ductility are realized for the smaller diameters while lower degradation rates exist for the mechanical properties of the higher diameters.

The yield stress (R_p), the uniform elongation (A_{gt}), and the energy density (U) for the non-corroded and for the 120 days corroded specimens were reduced as follows:

Rebar diameter, mm	$R_{p\text{-}nom}$, %	A_{gt}, %	U, %
8	31	66	73
18	10	24	22

Knowing that the energy density and yield stress characterize the quality index of the material (Ref 21), it appears that the mechanical performance of steel reinforcement, corroded or not, is not constant for all diameters.

Figure 11 shows that the energy density, representing the energy reserves of the various diameters specimens, coincides only in a region of approximately 10-20 days corrosion level.

Figures 8 and 9 indicates that the uniform elongation limit might fluctuate from 14.53% for the non-corroded 18 mm diameter specimens to 3.50% for the highly corroded 8 mm diameter. A similar situation is to be expected in a reinforced concrete member, where corrosion is going to attack initially the smaller diameter reinforcing steel, usually found in the outer beam and column stirrups, while the larger diameter may remain unharmed. In actual practice, where corrosion takes place under stress corrosion cracking conditions, the worst-case scenario is to be expected. The scattering of values in the mechanical performance of $B500_c$ steel in reinforced concrete structures, under marginal loading conditions, might lead to unpredictable performance with negative consequences for the structural integrity.

Existing design codes for reinforced concrete structures do not take into consideration the variation of the mechanical properties of $B500_c$ steel due to diameter variation or material specifications (Ref 17-20, 22). Corrosion and size variation of the steel reinforcement must be seriously regarded in new construction.

Table 3 Approximation constants used in the nonlinear fitting of the mechanical properties

Constants	Extreme value U	Polynomial				
		$R_{p\text{-}nom}$	$R_{m\text{-}nom}$	$R_{p\text{-}eff}$	$R_{m\text{-}eff}$	A_{gt}
a	84.420	670.121	749.809	594.976	653.894	8.318
b	24.078	−2.0550	−2.1495	−1.0344	0.9845	−0.0868
c	2.620	−7.9088	−1.9628	2.03020	10.348	0.12712
d	35.065	0.00038	0.00059	0.000562	0.001482	0.00014
e	52.084	0.18432	−0.01478	−0.20291	−0.4785	0.01132
f	5.953	0.08394	0.0887	0.049180	0.03818	0.0025
g	4.700					
h	68.383					

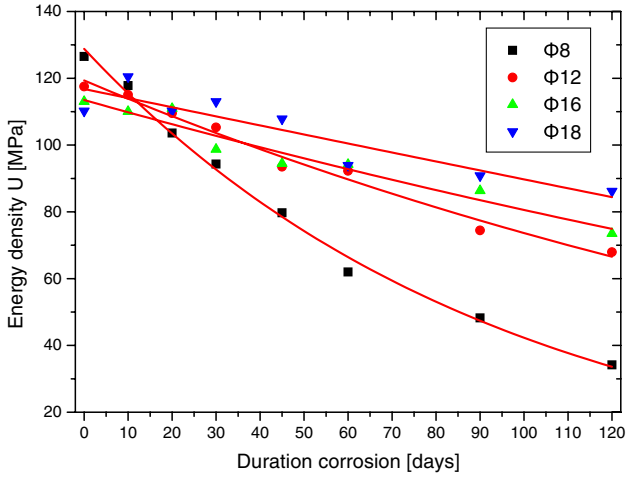

Fig. 11 Rate of change of the energy density as a function of the corrosion duration and diameter size

5. Conclusion

An experimental study was conducted in order to evaluate the impact of corrosion on the tensile mechanical properties and gauge variation of $B500_c$ steel rebar, and the following conclusions are drawn:

1. The mechanical properties depend upon the rebar cross-sectional area size and level of corrosion.
2. The rate of change of the mechanical properties of $B500_c$ steel rebar during accelerated salt spray corrosion is not equal for all size rebar. The variation of the mechanical properties for the larger diameter rebar appears to be smaller than the corresponding values for smaller diameter specimens.
3. The variation of strength and ductility mechanical properties vs. rebar size of $B500_c$ steel must be re-evaluated and further research should be encouraged in order to gain additional knowledge for more effective design.

References

1. J.P. Broomfield, *Corrosion of Steel in Concrete*. E & FN Spon., London, 1997, p 22
2. V.G. Papadakis, Supplementary Cementing Materials in Concrete—Activity, Durability and Planning. Danish Technological Institute Concrete Center, January 1999
3. R. Capozucca, Damage to Reinforcement Concrete due to Reinforcement Corrosion, *Constr. Build. Mater.*, 1995, **9**(5), p 295–303
4. M.G. Alvarez and J.R. Galvele, The Mechanisms of Pitting of High Purity Iron in NaCl Solutions, *Corros. Sci.*, 1984, **24**, p 27–48
5. G.K. Glass and N.R. Buenfeld, Chloride-Induced Corrosion of Steel in Concrete, *Prog. Struct. Eng. Mater.*, 2000, **2**(4), p 448–458
6. C. Fang, K. Lundgren, L. Chen, and C. Zhu, Corrosion Influence on Bond in Reinforced Concrete, *Cement Concrete Res.*, 2004, **34**(11), p 2159–2167
7. A. Ouglova, Y. Berthaud, M. François, and F. Foct, Mechanical Properties of an Iron Oxide Formed by Corrosion in Reinforced Concrete Structures, *Corros. Sci.*, 2006, **48**(12), p 3988–4000
8. J.P. Broomfield, *Corrosion of Steel in Concrete: Understanding, Investigation and Repair.* St. Edmundsbury Press Limited, Bury St. Edmunds, Suffolk, 1997
9. A.A. Almusallam, A.S. Al-Gahtani, A.R. Aziz, and Rasheeduzzafar, Effect of Reinforcement Corrosion on Bond Strength, *J. Constr. Build. Mater.*, 1996, **10**(2), p 123–129
10. A.A. Almusallam, A.S. Al-Gahtani, A.R. Aziz, F.H. Dakhil, and Rasheeduzzafar, Effects of Reinforcement Corrosion on Flexural Behavior of Concrete Slabs, *J. Mater. Civil Eng.*, **8**(3), p 123–127
11. C.A. Apostolopoulos, M.P. Papadopoulos, and Sp.G. Pantelakis, Tensile Behaviour of Corroded Reinforcing Steel Bars $BSt500_s$, *J. Constr. Build. Mater.*, 2006, **20**, p 782–789
12. C. Apostolopoulos and D. Michalopoulos, Impact of Corrosion on Mass Loss, Fatigue and Hardness of BSt500s Steel, *J. Mater. Eng. Perform.*, 2007, **16**(1), p 63–67
13. Ch.Alk. Apostolopoulos and D. Michalopoulos, The Effect of Corrosion on the Mass Loss and Low Cycle Fatigue of Reinforcing Steel, *J. Mater. Eng. Perform.*, 2006, **15**(6), p 742–749
14. C. Apostolopoulos, Mechanical Behavior of Corroded Reinforcing Steel Bars S500s tempcore under Low Cycle Fatigue, *Constr. Build. Mater.*, 2007, **21**, p 1447–1456
15. C.A. Apostolopoulos and M.P. Papadopoulos, Tensile and Low Cycle Fatigue Behavior of Corroded Reinforcing Steel Bars S400, *J. Constr. Build. Mater.*, 2007, **21**, p 855–864
16. M.G. Fontana, *Corrosion Engineering*. 3rd ed., McGraw-Hill, New York, 1987
17. Hellenic Regulation for the Technology of Steel in Reinforced Concrete, No Δ14/36010-29.2/24.3.2000 (Government Gazette Issue), 381B (in Greek)
18. EAK 2000, Ministry of Environment Planing and Public Works, Greek Earthquake Resistant Design Code. Athens, 2000 (in Greek)
19. FEMA-310, 1998, *Handbook for the Seismic Evaluation of Buildings: A Prestandard*, prepared by the American Society of Civil Engineers for the Federal Emergency Management Agency, Washington, DC
20. Steel for Reinforcement of Concrete—Weldable Ribbed Reinforcing Steel B500—Technical Delivery Condition for Bars, Coils and Welded Fabric prEN 100080/95
21. M. Papadopoulos, C. Apostolopoulos, N. Alexopoulos, and S. Pantelakis, Effect of Salt Spray Corrosion Exposure on the Mechanical Performance of Different Technical Class Reinforcing Steel Bars, *Mater. Des.*, 2007, **28**(8), p 2318–2328
22. ELOT 1421, Hellenic Standard Steel for the Reinforcing of Concrete—Weldable Reinforcing Steel—Part 1, 2, 3: Technical class $B500_c$, Athens, 2004